Active Site Control of Myosin Cross-Bridge Zeta Potential†

William Bernt,‡,§ Katherine Polosukhina,‡,|| Bruce Weiner,§ Walther Tscharnuter,§ and Stefan Highsmith*,||

Department of Biochemistry, University of the Pacific School of Dentistry, San Francisco, California 94115-2399, and Research Division, Brookhaven Instrument Corporation, Holtsville, New York 11742-1832

Received April 22, 2002; Revised Manuscript Received July 12, 2002

ABSTRACT: The electrical properties of contractile proteins contribute to muscle structure and perhaps function but have not been characterized adequately. Electrophoretic mobility, μ_e, is sensitive to the net electric charge and hydrodynamic size of a molecule in solution. Zeta potential, ζ, particle charge, Q_e, and particle charge-to-mass ratio are proportional to μ_e. We measured μ_e for nucleotide complexes of skeletal muscle heavy meromyosin (HMM) and subfragment 1 (S1). The results indicate that μ_e for HMM changes depending on the ligand bound in the active site. The changes in electric charge appear to occur mainly on the S1 moieties. For HMM(MgATPγS)$_2$ and HMM(MgADP·P$_i$)$_2$ the values of μ_e are -0.077 and -0.17 (μm/s)/(V/cm), respectively. For these complexes, μ_e is independent of [ATP], [ADP], and [P$_i$]. When P$_i$ dissociates from HMM(MgADP·P$_i$)$_2$ to form HMM(MgADP)$_2$, μ_e decreases to -0.61 (μm/s)/(V/cm). This large decrease in μ_e is independent of free [ADP] or [ATP]. Increasing [P$_i$], on the other hand, increases μ_e for HMM(MgADP)$_2$ to values near those observed for the steady-state intermediate. For HMM, $\mu_e = -0.34$ and is independent of P$_i$. MgADP binding to HMM decreases μ_e to -0.57 (μm/s)/(V/cm), and the dissociation constant is 9 μM. Taken together, these data indicate that μ_e and, thus, ζ are controlled by ligand binding to the active site. The magnitudes of the particle charge-to-mass ratios for the HMM complexes are all in a range that falls within published values determined for a variety of other proteins. Possible roles that the observed nucleotide-dependent changes in cross-bridge electric charge might have in the contractile cycle in muscle are considered.

Skeletal muscle structure is sensitive to the electrical properties of myosin and actin. The thin and thick filaments have a net negative charge that generates electrostatic repulsion (*1*, *2*). As a result, in relaxed and contracting muscle, the hexagonal arrays of filaments are under repulsive stress (*3*), and the ATP hydrolysis-driven contractile cycle occurs in the electric field of the filaments. More recently, it has been shown that mammalian skeletal muscle thick filaments have negatively charged motor domains that are longer than the thick-to-thin surface-to-surface interfilament distance, so that the motor domains extend azimuthally from the thick filament surface into space between neighboring thin filaments (*4*, *5*). This spatial arrangement makes it likely that motor domain position is sensitive to changes in net electric charge on either filament (Figure 1A). If these electrostatic interactions have a functional role, then changes in electric charge on the thick filament, particularly on the myosin motor domain, should be coupled to the ATP hydrolysis cycle and be nucleotide-dependent.

Information on myosin motor domain electrical properties is scarce. Donnan potential measurements on gels of intact myosin indicate that large decreases in negative surface charge occur when ATP is added (*6*). The data suggest that ATP causes a decrease of 30−40 |e| per myosin, due in part to increased binding of anions other than ATP. This is a remarkably large change in myosin electric charge, which could affect muscle fiber structure and/or function. But to begin to interpret this result, one must know where on myosin the change occurs. To this end, we have measured electrophoretic mobility and hydrodynamic size of nucleotide complexes of heavy meromyosin (HMM),[1] a soluble proteolytic fragment of myosin, which includes two motor domains connected to a portion of the coiled coil of α-helices, and of subfragment 1 (S1), the isolated motor domain (Figure 1B).

Electrophoretic mobility, μ_e, in solution depends on the net electric charge density at the shear plane (zeta potential, ζ) of a particle or molecule in the presence of an applied electric field. Phase analysis light scattering, PALS, was used to measure μ_e (*31*, *32*). At constant temperature, if the electric charge increases or the hydrodynamic size decreases, the mobility of the molecule in the electric field increases. Changes in electric charge for the molecule can be due to changes in surface charge and/or changes in counterion binding within the shear plane. Changes in hydrodynamic size are due to conformational changes and need to be measured independently. Dynamic light scattering, DLS, measures the rate of Brownian motion by photon correlation spectroscopy, which can be used to calculate a mean effective diameter, *d*(eff), for the molecule or to determine a size distribution (*7*).

† Supported by NIH Grant AR42895.

* Address correspondence to this author. Tel: 415-929-6670. Fax: 415-929-6654. E-mail: shighsmith@sf.uop.edu.

‡ W.B. and K.P. contributed equally to this work.

§ Brookhaven Instrument Corp.

|| University of the Pacific School of Dentistry.

[1] Abbreviations: HMM, heavy meromyosin; S1, myosin subfragment 1; ATPγS, adenosine 5′-γ-thiotriphosphate; μ_e, electrophoretic mobility; Q_e, particle charge; ζ, zeta potential.

10.1021/bi0202979 CCC: $22.00 © 2002 American Chemical Society
Published on Web 08/22/2002

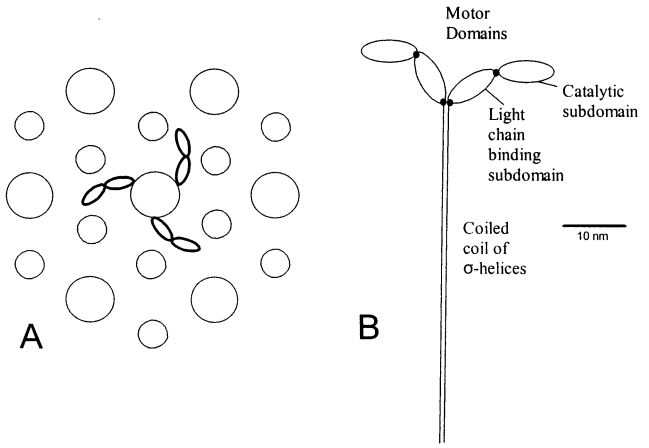

FIGURE 1: Schematic structures. (A) A cross section of skeletal muscle A-band shows the crowded hexagonal arrangement of the filaments. The core diameters of the thick and thin filaments are 16 and 10 nm, respectively, and their surfaces are 12 nm apart, based on X-ray diffraction experiments on skinned fibers (*5*). The 19 nm motor domains of three myosin molecules are shown protruding from one thick filament at azimuthal angles. For clarity, only one of the two motor domains that are part of each myosin cross-bridge is shown. All the surfaces have net negative electric charge (*48*). (B) The 350 kDa soluble proteolytic fragment of myosin called heavy meromyosin (HMM) has two 19 nm long motor domains (each depicted as two ovals connected by a black dot) connected to a 58 nm long coiled coil of α-helices. Each motor domain has a catalytic subdomain that binds actin and ATP and a light chain-binding subdomain that is thought to move as a lever arm during contraction. The black dots represent sites of flexible linkage. The coiled-coil region behaves hydrodynamically as a rigid rod. The parent molecule myosin has an ~70 nm extension of the coiled coil, which induces myosin to aggregate into thick filaments.

An individual motor domain contains the actin and ATP binding sites. It can generate force in the presence of actin (*8*) and has been intensely studied. Structures have been solved for several nucleotide complexes of intact motor domain (*9*−*11*) and of a truncated catalytic subdomain (*12*−*16*), which have led to hypotheses of force generation by movement of a lever arm subdomain of the motor domain. The structural and kinetic aspects of motor domain force generation are reviewed frequently (*17*−*20*), although possible roles of the negative potential due to the filament surface charge are usually ignored. HMM is a more complex structure, and results obtained with it are more difficult to interpret. But HMM is the myosin construct used most often for in vitro assays of motility and force (*21*). It retains structural properties required for processivity (*22*) and regulation in several nonskeletal myosins (*23*, *24*), which are lost when the motor domain is isolated.

The effects of ATP, ADP, and P_i and of the analogue of unhydrolyzed ATP, ATPγS, on μ_e and d(eff) were determined for HMM and S1 in solution at 20 °C. There are many advantages to being able to characterize the properties of purified molecules in solution, where the conditions can be manipulated and the data analyzed using physical chemical theory. The values of μ_e were used to estimate zeta potentials, ζ, and particle charges, Q_e. The results indicate that the HMM portion of myosin has a net negative charge and that its magnitude is dependent upon the ligand bound at the active site. The most striking result is that the net charge is much more negative when P_i dissociates from HMM(MgADP·P_i)$_2$ to produce HMM(MgADP)$_2$. Comparable nucleotide-dependent changes in electric charge were observed for S1, suggesting that the P_i-induced HMM electric charge increase occurs mainly on the motor domains.

MATERIALS AND METHODS

Proteins and Chemicals. Myosin was isolated from rabbit skeletal muscle (*25*). HMM was prepared from myosin using TLCK-treated α-chymotrypsin (Sigma) in the presence of Mg^{2+} (*26*) and further purified by size exclusion chromatography using Sephacryl S-300. S1 with both light chains present was prepared from myosin using papain in the presence of Mg^{2+} (*27*) and purified on Sephacryl S-400. The specific steady-state ATPase activities at 20 °C were 0.07−0.10 s^{-1} for HMM and 0.035−0.042 for S1, using Malachite green to determine P_i production (*28*) or using a coupled assay to detect ADP production (*29*). Commercial reagent grade chemicals were used without further purification, except for ATPγS, which was purified by ion-exchange chromatography (*30*).

Phase Analysis Light Scattering. The instrument has been described (*31*). In a PALS experiment the scattered light at 15° is mixed with a reference beam that is phase shifted by a digitally controlled mirror. The scattered signal is phase shifted relative to the reference signal to a degree that is determined primarily by the average positions of the particles. If the particles move under the force of an applied electric field, the phase difference changes. The average electrophoretic mobility, $\langle\mu_e\rangle$, is determined from the measured phase difference. PALS is well suited for measuring small zeta potentials, which are expected for individual molecules (*32*).

The theoretical basis of the PALS analysis is too lengthy to include here in detail (*32*), but it is useful to consider the equation

$$\Delta\phi(t) = \langle\mu_e\rangle(\vec{q}\cdot\vec{E}_0)\cos(\omega_E t)/\omega_E + (\vec{q}\cdot\vec{V}_c)t \qquad (1)$$

in which $\Delta\phi(t)$ is the measured, amplitude-weighted phase difference; $\vec{q}$ is the scattering wave vector; $\vec{E}_0$ is the applied electric field; ω_E is the frequency at which the field is oscillated; $\vec{V}_c$ is any field-independent drift velocity, e.g., convection. The magnitude of the scattering wave vector, q, is calculated from the refractive index, n, of the liquid, the wavelength of the laser, λ_0, and the scattering angle, θ, as follows:

$$q = (4\pi n/\lambda_0)\sin(\theta/2) \qquad (2)$$

Data (see Figure 2) are fitted to eq 1 to determine $\langle\mu_e\rangle$ and V_c, the magnitude of the drift velocity, of which only $\langle\mu_e\rangle$ is important. Compared to conventional laser Doppler electrophoresis methods, PALS has the advantages of allowing one to measure smaller particles, with lower mobilities, using smaller electric fields, which makes it possible to investigate the electrical properties of HMM in the 5 μM range. Accuracy was validated using the electrophoretic mobility standard goethite (α-FeOOH) in phosphate−perchlorate (pH 2.5), supplied by NIST. The PALS measured value was $\mu_e = 2.54 \pm 0.05$ (μm/s)/(V/cm) and the NIST SRM1980 value was 2.53 ± 0.12 (μm/s)/(V/cm).

Electrophoretic Mobility Measurements. In a typical experiment, the ligand was added last from a concentrated

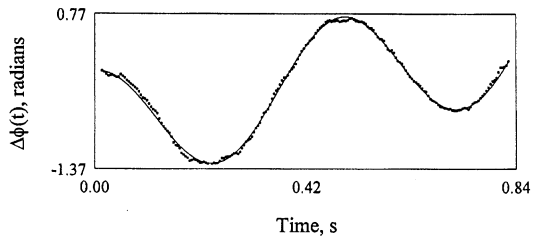

FIGURE 2: Amplitude-weighted phase shift difference data. A plot of $\Delta\phi(t)$ versus t for 5 μM HMM(MgADP)$_2$ in 5 mM Mops (pH 7.0), 1 mM KOAc, 1.0 mM MgADP, and 0.6 mM $MgOAc_2$ at 20 °C after 50 cycles of an applied 10.7 V/cm electric field is typical. The solid line is the fit of eq 1 to the data to determine μ_e (see Materials and Methods).

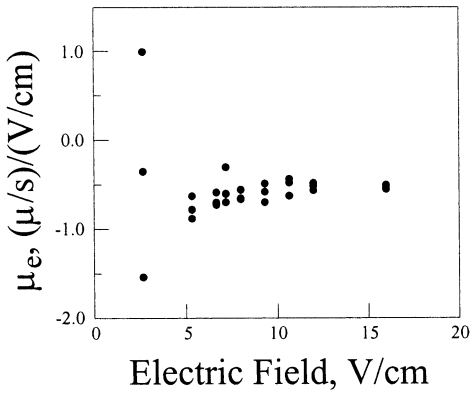

FIGURE 3: Electric field strength dependence of μ_e. The electrophoretic mobility of HMM(ADP)$_2$ was measured for field strengths between 2.2 and 16 V/cm to determine the minimum field that will give reliable results for a 50-cycle measurement. The data in Table 1, and in Figures 4, 6, 7, and 8, were collected using field strengths above 7 V/cm.

stock solution to obtain 2.0 mL of sample that was passed through a syringe-mounted 0.45 μm filter directly into a cuvette. The electrode was inserted into the cuvette, and the assembly was placed in a temperature-controlled cell holder. To minimize the time between adding a reactive ligand and the first measurement of a time-dependent series, the stock solutions and buffers were preequilibrated at 20 °C before the mixing, filtering, and loading procedure. This procedure enabled data collection to begin within 5 min of adding ATP or ATPγS to the HMM solution.

Data were collected in runs consisting of some number of cycles of exposure to the applied electric field. The wavelength of the incident light was 676 nm. The laser intensity was 30 mW. With 5 μM HMM samples, the signal-to-noise ratio for a run was satisfactory after 25 cycles (~70 s). Typically 50 cycles were collected per run, but results for runs with from 25 to 200 cycles are reported here. Because HMM is vulnerable to damage when exposed to an electric field (*33*), control experiments were done to determine a useful electric field strength range that provides reproducible data without damage to the sample. The field strength dependence of the electrophoretic mobility of HMM-(MgADP)$_2$ indicates that, for 50-cycle runs, fields above 6 V/cm produce data that are reliable (Figure 3). For HMM in the presence of P_i, ADP, and ATP, repeated PALS measurements of μ_e could be made using fields as high as 12 V/cm with no detectable aggregation or loss of MgATPase activity. The experimental error was larger for measurements made on HMM in the absence of nucleotide, although there was no measurable loss of activity. Samples containing ATPγS are more susceptible to electro- and/or photochemical degradation due to some combination of field strength, laser strength, and [ATPγS]. By reducing [ATPγS] to 0.5 mM (compared to 1−5 mM for other ligands) and keeping the electric field below 8 V/cm, samples are stable enough to make several runs over a 1 h period.

One experimental approach was to measure the time dependence of μ_e for HMM in the presence of the substrates ATP and ATPγS. They form steady-state intermediates that persist for from 30 to 60 min under the conditions used. The time required for a 50-cycle run is 2.3 min, allowing time for adequate sampling before and after substrate is exhausted. Typically five or fewer measurements were made at varied increasing times on a sample to avoid damage, and data for several samples were combined. When HMM and ATP are incubated at 4 °C for 16 h to convert all ATP to ADP and P_i, the electrophoretic mobility at 20 °C is the same, within experimental error, as observed for an identical sample for which measurements were made at 20 °C after ATP hydrolysis was complete. This control measurement indicates that neither the electric field nor the laser irradiation affects the mobility during a typical 2 h measurement period. The MgATPase activity of HMM samples after three measurements of 50-cycle runs is undiminished, within experimental error, compared to an identical sample that was not used for measurements, confirming that HMM is not modified detectably by the PALS measurements.

Particle Sizing. Particle size measurements on HMM were made by conventional dynamic light scattering techniques (*7*, *34*). The data were used to calculate the effective diameter, d(eff), of a spherical particle with equivalent hydrodynamic mobility (*34*).

Simulation of ATPase Kinetics. One of the products of HMM hydrolysis of ATP and ATPγS is ADP, which is a competitive inhibitor of HMM activity. An integrated rate equation cannot be solved for [HMM(ADP·P_i)$_2$] or [ADP] at all times, when there is competitive product inhibition (*35*). To calculate the time dependence of the transition from HMM−substrate to HMM−product, a kinetic simulation was made using the equation

$$E + S \overset{K_S}{\longleftrightarrow} ES \overset{k}{\rightarrow} EP \overset{K_P}{\longleftrightarrow} E + P \qquad (3)$$

in which E = HMM, S = MgATP or MgATPγS, P = MgADP, k is the steady-state specific rate for the reaction in the presence of excess substrate, K_S = [E][S]/[ES], and K_P = [E][P]/[EP]. Assuming that E_0 = ES + EP, substitution of K_S and K_P followed by rearrangement gives

$$[ES] = E_0/\{1 + ([P]/[S])(K_S/K_P)\} \qquad (4)$$

which can be used to calculate [ES] at any time, if [S], [P], K_S, and K_P are known at that time.

A simulation was done as follows. At t = 0, [P] = 0, so [ES] = E_0 and the early steady-state rate is kE_0. After a suitably small arbitrary increment of time, Δt, [S] = $S_0 - kE_0\Delta t$ and [P] = S_0 − [S], which are substituted, along with values for K_S and K_P, into eq 4 to calculate [ES] at the end of the increment. This process is repeated, using a smaller time increment for each iteration, to obtain [ES] at increasing times until it is arbitrarily close to zero. Values of K_S =

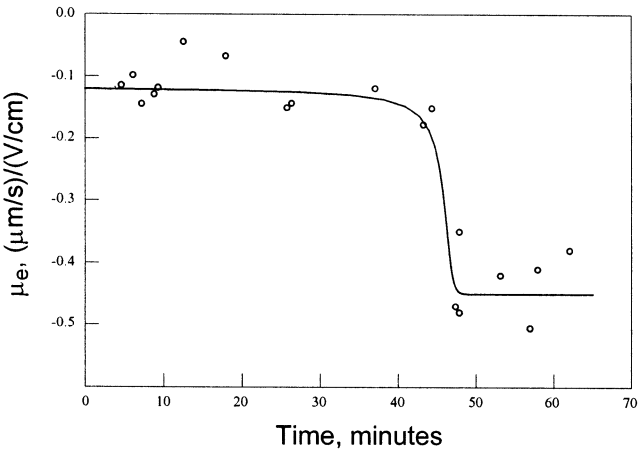

FIGURE 4: Time dependence of HMM electrophoretic mobility in the presence of ATP. At $t = 0$, 1.0 mM MgATP was added to 5.0 μM HMM in 5.0 mM Mops (pH 7.0), 1 mM KOAc, and 0.60 mM $MgOAc_2$ at 20 °C. μ_e was measured over times sufficient to convert all of the ATP to ADP and P_i. Data points are 25 or 50 cycles per run. The solid line was obtained using eq 4 to simulate [HMM-(MgADP·P_i)$_2$] and [HMM(MgADP)$_2$], which were assigned μ_e values of -0.12 and -0.45 (μm/s)/(V/cm), respectively, for 5.0 μM HMM and 1.0 mM MgATP; MgATPase = 0.077 s^{-1}, $K_S = 10^{-8}$ M, and $K_P = 10^{-6}$ M (see text). The decrease in μ_e is cotemporaneous with P_i dissociation.

10^{-8} M and $K_P = 10^{-6}$ M were used, but similar results are obtained whenever $K_S/K_P \ll 1$.

RESULTS

Electrophoretic Mobility of HMM Complexes. The electrophoretic mobility of 5−7.5 μM HMM in the presence of 1.0 mM MgATP was measured at increasing times over periods long enough to convert ATP to ADP and P_i. At early times, when the steady-state intermediate HMM(MgADP·P_i)$_2$ is present, $\mu_e = -0.17 \pm 0.07$ (μm/s)/(V/cm). When the ATP is exhausted and HMM(MgADP)$_2$ is present (Figure 4), μ_e decreases (all HMM μ_e are negative, so numerical decreases in μ_e indicate increases in mobility and in negative charge) to -0.47 ± 0.10 (μm/s)/(V/cm) [μ_e for HMM-(MgADP)$_2$ is lower when P_i is absent; Table 1]. The time at which the transition occurs is simulated using eq 4 and the known [HMM], [ATP], and MgATPase activity (Figure 4), which is consistent with a strong correlation of the decrease of μ_e and the transition from HMM(MgADP·P_i)$_2$ to HMM-(MgADP)$_2$. When [MgATP] is increased to 2.0 mM, μ_e is unchanged at early times, but the time at which μ_e decreases is doubled (data not shown). These results are consistent with the observed decrease in μ_e occurring when P_i dissociates from HMM(MgADP·P_i)$_2$.

The possibility that the observed decrease in μ_e is due to P_i binding to HMM(MgADP·P_i)$_2$ or HMM(MgADP)$_2$ as it increases from 0 to 1 mM during ATP hydrolysis was examined by measuring μ_e for HMM in the presence of nucleotides with increasing added [P_i]. For HMM in the absence and presence of 1.0 mM P_i, μ_e was -0.34 ± 0.11 and -0.33 ± 0.09 (μm/s)/(V/cm), respectively. A decrease of less that 0.1 (μm/s)/(V/cm) for the value of μ_e was observed for HMM(MgADP·P_i)$_2$ when [P_i] was increased from 0 to 3 mM (Figure 5). In contrast, added P_i had a striking effect on HMM(MgADP)$_2$, increasing μ_e to the level observed for the steady-state intermediate (Figure 6). These data suggest that nonspecific binding of P_i to HMM has little effect on μ_e. In contrast, P_i binding to HMM(MgADP)$_2$ reverses the decrease in μ_e observed when P_i dissociates from the active site (Figure 6), presumably by binding to the vacant phosphate binding subsite of the active site.

The binding of ADP to HMM decreases μ_e from -0.34 ± 0.11 to -0.61 ± 0.11 (μm/s)/(V/cm). The value of μ_e is lower in this case than at the end of an ATP hydrolysis measurement (Figure 4) because there is no P_i present. When the concentration dependence of the decrease was fitted to an equation for equilibrium binding, $K_D = (9 \pm 13) \times 10^{-6}$ M (Figure 7). The uncertainty of the fitted parameter is large, but the value of K_D is consistent with ADP binding to the active site (*36*). These ADP data confirm that μ_e is modulated by ligand binding.

The ATP analogue ATPγS is a substrate for HMM, but the steady-state intermediate has the unhydrolyzed form of the substrate, rather than the products, bound in the active site (*37*, *38*). When ATPγS is added to HMM, μ_e is -0.077 ± 0.03 (μm/s)/(V/cm) at the early times when HMM-(MgATPγS)$_2$ is present and decreases to -0.56 ± 0.16 (μm/s)/(V/cm) after ATPγS is hydrolyzed. The data suggest that thiophosphate has less effect than phosphate on μ_e. The values of μ_e for the above HMM intermediates are summarized in Table 1.

Hydrodynamic Size of HMM Complexes. The observed decrease in μ_e that occurs when P_i dissociates from HMM-(MgADP·P_i)$_2$ (Figure 4) could be due in part to decreased hydrodynamic size. DSL measurements of *d*(eff) were made for HMM at increasing times after the addition of ATP in solutions identical to those used for the μ_e measurements. At early times, *d*(eff) for HMM(MgADP·P_i)$_2$ is 24.1 ± 1.6 nm, and at later times, when HMM(MgADP)$_2$ is present, *d*(eff) increases to 31.9 ± 2.5 nm (Figure 8). As was the case for the decrease in μ_e (Figure 4), simulation of the time dependence of [HMM(MgADP·P_i)$_2$] using eq 4 indicates that the increase in *d*(eff) occurs when ATP was exhausted.

HMM has motor domains connected to the coiled coil by flexible linkages (*39*), making assignment of the *d*(eff) values to specific structures difficult. The calculated diameter of a sphere of equivalent mass is 10.4 nm (assuming 3 g of water/g of protein), while the longest HMM dimension approaches 80 nm (Figure 1). Nonetheless, the observed *d*(eff) values are useful here as measures of relative hydrodynamic size. The data confirm that when P_i dissociates, μ_e decreases because of increased negative charge rather than decreased hydrodynamic size. The increase in *d*(eff) makes the magnitude of the observed decrease in μ_e a lower limit (Table 1). HMM(MgADP)$_2$ may be larger due to increased electrostatic repulsion between the flexibly attached motor domains and/or the coiled-coil region, which favors motor domains positioned in more expanded conformations, or it may be due to a ligand-induced conformational change to a hydrodynamically larger particle. The mechanism for the increase in size was not investigated further.

Electrophoretic Mobility and Hydrodynamic Size of S1 Complexes. The effect of ATP hydrolysis on μ_e was measured for S1 in the same buffer used for HMM. For S1·MgADP·P_i, $\mu_e = -0.14 \pm 0.05$ (μm/s)/(V/cm). It decreases to -0.41 ± 0.10 (μm/s)/(V/cm) for S1·MgADP in the presence of 1 mM P_i. The decrease for S1 is comparable to that for HMM (Table 1), consistent with the HMM change in electrical charge occurring on the motor domains. DLS

Table 1: Electrophoretic Mobilities and Zeta Potentials for HMM and S1 Complexes[a]

complex	μ_e, (μm/s)/(V/cm)	n	ζ, mV	Q_e, |e|	$Q_e/M^{2/3}$, |e|/$D^{2/3}$
HMM	-0.34 ± 0.11	10	-4.8 (-7.2)	-19 (-28)	-0.0038 (-0.0057)
HMM-ATPγS	-0.077 ± 0.03	9	-1.1 (-1.6)	-4.3 (-6.5)	-0.0009 (-0.0014)
HMM-ADP·P_i	-0.17 ± 0.08	14	-2.4 (-3.6)	-9.3 (-14)	-0.0019 (-0.0029)
HMM-ADP	-0.61 ± 0.11	9	-8.6 (-12.9)	-34 (-50)	-0.0067 (-0.010)
S1-ADP·P_i	-0.14 ± 0.05	7	-2.0 (-3.0)	-7.8 (-12)	-0.0030 (-0.0045)
S1-ADP ($+P_i$)	-0.41 ± 0.10	7	-5.8 (-8.7)	-23 (-34)	-0.0086 (-0.013)

[a] Electrophoretic mobilities, μ_e, were measured for 5.0−7.5 μM HMM or S1 at 20 °C in 5.0 mM Mops (pH 7.0), 1.0 mM KOAc, 0.60 $MgOAc_2$, and 1.0 mM Mg−ligand to form a complex (except [MgATPγS] = 0.50 mM). Values are averages for n runs of 25−200 cycles. Zeta potentials, ζ, were calculated using the Smoluchowski equation, $\mu_e = \epsilon_0\epsilon_r\zeta/\eta$, and the Huckel equation $\mu_e = {}^2/_3\epsilon_0\epsilon_r\zeta/\eta$ (in parentheses), where ϵ_0 is the permittivity of light in a vacuum, ϵ_r is the relative dielectric constant for water, and η is the viscosity of water at 20 °C. The particle charge, Q_e, was calculated from ζ using the equation $Q_e = 4\pi\epsilon_0\epsilon_r a(1 + \kappa a)\zeta$ (SI units are used here; see ref *47*, pp 357−359). The charge−mass ratios are given as $Q_e/M^{2/3}$ for comparison to existing tabulated data for other proteins (*42*). Values in parentheses were calculated using Huckel ζ's.

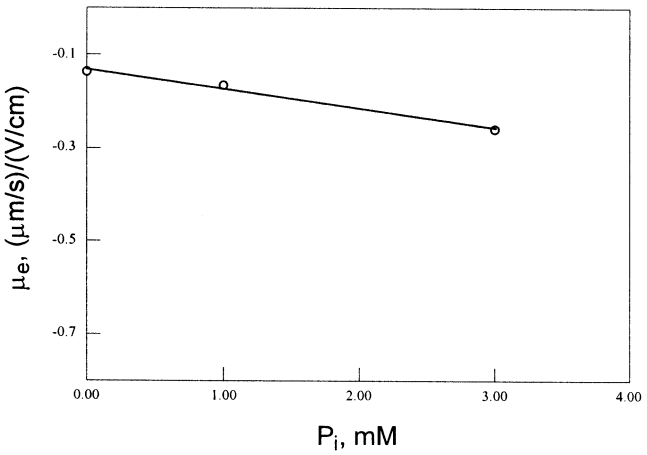

FIGURE 5: Dependence on added free phosphate of μ_e for HMM-$(MgADP{\cdot}P_i)_2$. ATP was added to HMM in solutions as described in Figure 4, except that additional P_i was included. μ_e was measured during the time that the steady-state intermediate was present. The small decrease in μ_e may be due to nonspecific binding of P_i to the complex or to increased ionic strength. The line is a linear fit to the data.

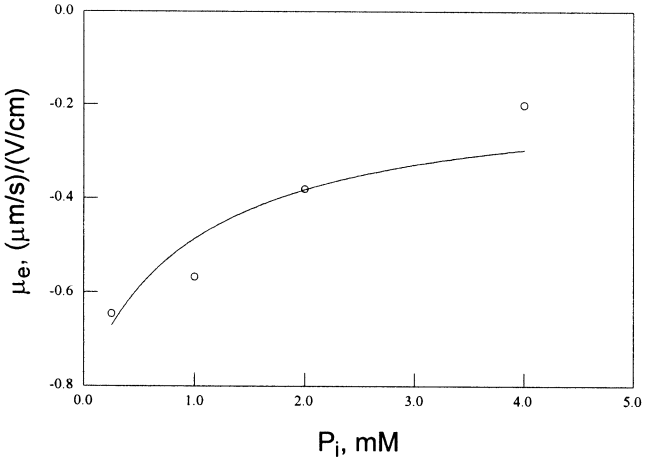

FIGURE 6: Dependence on added free phosphate of μ_e for HMM-$(MgADP)_2$. ATP was added to HMM in solutions as described in Figure 4, except that additional P_i was included. μ_e was measured during times after the ATP was exhausted and $HMM(MgADP)_2$ was present. The large increase in μ_e suggests that P_i binds to HMM-$(MgADP)_2$ and decreases the negative charge of the complex. The solid line is a fit to the data for P_i binding assuming that it binds $HMM(MgADP)_2$ in a simple equilibrium and that μ_e is -0.12 (μm/s)/(V/cm) for $HMM(MgADP{\cdot}P_i)_2$. The fitted values were $K_D = (1.1 \pm 0.7) \times 10^{-3}$ M and $\mu_e = -0.75 \pm 0.18$ (μm/s)/(V/cm) for $HMM(MgADP)_2$, consistent with P_i binding at the active site. The fitted value of μ_e is lower than the values measured after ATP is converted to ADP in Figure 4 because P_i is present in the experiments in Figure 4.

measurements on S1·nucleotide complexes indicate that d(eff) = 10.5 ± 0.3 and 11.0 ± 0.2 nm for S1·MgADP·P_i and S1·MgADP, respectively (data not shown), consistent with previous results (*34*). As for HMM, the decrease in μ_e when P_i dissociates from S1·MgADP·P_i is due to increased negative charge, not decreased hydrodynamic size.

Calculations of HMM and S1 Electrical Properties. Zeta potentials, ζ, were calculated for the HMM and S1 complexes from the experimentally determined electrophoretic mobilities (Table 1). It is not obvious whether it is better to use the method of Smoluchowski or of Huckel, which is applicable when the ionic atmosphere surrounding the particle is small or large, respectively, compared to the radius of the particle. A quantitative test for the appropriate equation is $\kappa a \gg 1$ for Smoluchowski and $\kappa a \ll 1$ for Huckel, where a = the radius of the particle and $1/\kappa$ is the Debye length (see ref *47*, pp 69−71). The values of a = 14 and 5.4 nm were used for HMM and S1, respectively, on the basis of the DSL measurements of the hydrodynamic radii. The Debye length, which is often taken as the thickness of the double layer of small ions that surround a charged particle, is 3.5 nm. Using these κ and a values, κa = 4 and 1.5 for HMM and S1, respectively. These are neither ≫1 nor ≪1, which reduces the certainty of the calculated values of ζ (*40*). Smoluchowski and Huckel values were calculated and provide a range of ζ values (Table 1). Because ζ is low in all cases, the two methods provide its upper and lower limits. In addition, any calculated ζ values for the HMM and S1 complexes must be considered to be estimates because of their asymmetric shapes (Figure 1). It is also true that the distribution of charge is not known, while the calculations of ζ are based on the assumption that charge is uniformly distributed on a spherical surface. Fortunately in this regard, recent experiments using the atomic structure of lysozyme to simulate values of ζ and calculate electrophoretic mobilities indicate that charge distribution is not very important (*41*). In summary, the calculated ζ values are less accurate than the μ_e values, because of the complex structures and solution conditions.

The net electric charge, Q_e, was calculated using the equation $Q_e = 4\pi\epsilon_0\epsilon_r a(1 + \kappa a)\zeta$, where ϵ_0 is the electric permittivity in a vacuum, ϵ_r is the relative dielectric constant for water, and a and κ have the definitions given above. These estimates of Q_e for HMM and S1 complexes were used to calculate the charge−mass ratio, $Q_e/M^{2/3}$, where M = 350000 Da and 135000 Da for HMM and S1, respectively (Table 1). For comparison, values of $Q_e/M^{2/3}$ that were

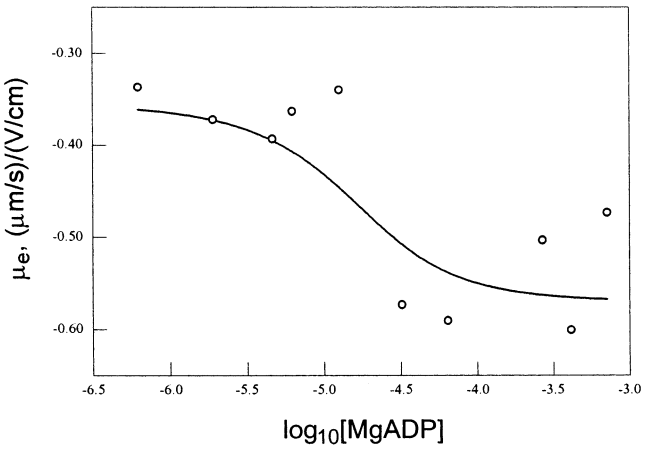

FIGURE 7: Changes in μ_e due to MgADP binding to HMM. μ_e was measured for HMM in the presence of increasing [MgADP]. The solid line is a fit to the data assuming ADP binding in a simple equilibrium and assigning $\mu_e = -0.36$ (μm/s)/(V/cm) for HMM. The fitted values for K_D and μ_e for HMM(MgADP)$_2$ are 9 ± 13 μM and -0.57 (μm/s)/(V/cm), respectively, consistent with MgADP binding to the active site.

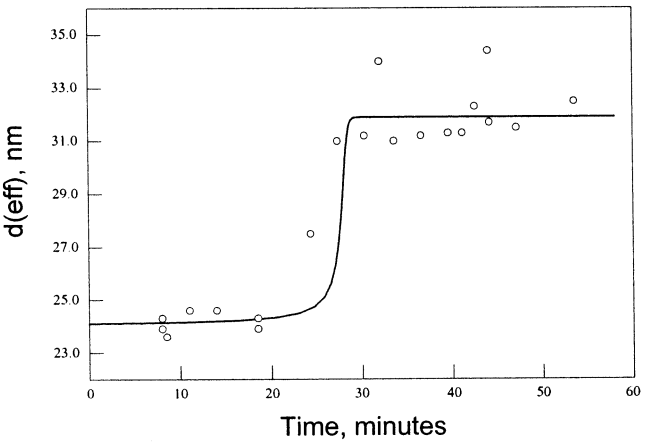

FIGURE 8: Time dependence of HMM hydrodynamic size in the presence of ATP. The conditions were identical to those in Figure 4. DLS was used to measure *d*(eff), the effective diameter of a sphere with a translational diffusion rate equal to the HMM complexes, at increasing times after the addition of ATP. The solid line was obtained using eq 4 to simulate [HMM(MgADP·P$_i$)$_2$] and [HMM(MgADP)$_2$], which were assigned *d*(eff) values of 24.1 and 31.9 nm, respectively, for 7.3 μM HMM and 1.0 mM MgATP; MgATPase = 0.084 s^{-1}, $K_S = 10^{-8}$ M, and $K_P = 10^{-6}$ M (see text). HMM hydrodynamic size increases when P$_i$ dissociates and μ_e decreases (Figure 4).

measured and tabulated for a large number of proteins have values that fall in the range -0.026 to $+0.027$ |e|/$D^{2/3}$ (*42*). The $Q_e/M^{2/3}$ values for HMM and S1 complexes fall in this range.

It is possible to estimate a limit for the value of Q_e at pH = 7 in the absence of any counterion binding from amino acid sequence data, assuming that all the Glu and Asp are -1 |e| and all the Lys and Arg are $+1$ |e|. Using skeletal muscle heavy and light chain sequences (*43*−*45*), the estimated upper limit is $Q_e = -78$ |e|. The measured values for HMM complexes (Table 1) are in the -4 to -50 |e| range.

DISCUSSION

This is the first characterization of the electrical properties of any isolated myosin cross-bridge, in this case rabbit skeletal muscle HMM in solution. The most interesting result is that μ_e for a HMM complex is determined by the ligand bound in the active site. In addition, the ligand-induced changes in μ_e for HMM are remarkably large. The values of ζ, Q_e, and $Q_e/M^{2/3}$ (Table 1) may be less accurate than μ_e, because of the assumptions made in their calculation (see above), but the relative values are useful. The $Q_e/M^{2/3}$ values calculated from the measured μ_e data (using the Smoluchowski ζ) for S1·MgADP·P$_i$ and S1·MgADP are -0.0030 and -0.0086 |e|/$D^{2/3}$, respectively. The comparable values for the corresponding HMM complexes are -0.0019 and -0.0067 |e|/$D^{2/3}$ (Table 1). The nearly equal decreases in charge-to-particle ratios and the larger magnitudes for the S1 complexes, in comparison to those for HMM, are consistent with the ligand-induced electric charge changes occurring on the motor domains of HMM. There is no need to evoke changes on the coiled-coil moiety.

The measurements of HMM hydrodynamic size were done as a control to ensure that the increase of μ_e when P$_i$ dissociates (Figure 4) is not due to a more compact HMM complex. The magnitude of the observed increase in size is somewhat surprising (Figure 8), although HMM has a unique and flexible structure that could assume conformations having a range of hydrodynamic mobilities. It is clear that the size increase and the electric charge increase occur when P$_i$ dissociates. The low ionic strength makes electrostatic repulsion a likely mechanism, but there is insufficient data to determine whether the size increase is caused by the charge increase.

The electrophoretic mobility measurements are consistent with Donnan potential measurements on skinned skeletal muscle fibers, which indicate that ATP increases thick filament negative charge (*48*). The present data localize the changes to the motor domains. They also suggest that the net negative electric charge is little changed by ATP hydrolysis but increases dramatically (~ -24 |e|) when P$_i$ dissociates. The change in particle charge calculated from μ_e for the HMM(MgADP·P$_i$)$_2$ to HMM transition is -9.4 |e| (Table 1), which is smaller than the charge difference of -30 to -40 |e| calculated from the Donnan potential change that occurs when ATP is added to myosin gels (*6*). The reason for the difference in the values for the change in electric charge is not clear. It may be due to contributions from the myosin structure that are absent from HMM, to differences in ionic strength, or to the assumption that HMM is a hard sphere used to calculate ζ.

Given the magnitude of the increase in negative electric charge, it is worthwhile considering possible artifacts for the HMM(MgADP·P$_i$)$_2$ to HMM(MgADP)$_2$ transition. P$_i$ dissociation would decrease the negative charge of an HMM complex, opposite of the observed increase. ATP is a stronger chelator of divalent cations than is ADP, so converting all of the free ATP to ADP might increase the free [Mg^{2+}], which, if bound to HMM, also would decrease its negative charge. The measurements were made in low [buffer], and ATP hydrolysis produces H^+, which could bind to HMM(ADP)$_2$ if it were competing with the buffer. But binding of H^+ to HMM(ADP)$_2$ also would decrease the negative electric charge. It is difficult to systematically eliminate all artifacts, but none of the obvious ones would contribute to an increase in negative electric charge.

The mechanism of the observed charge changes is of interest. Donnan potential measurements suggest that Cl^-

binding causes the increased negative charge on myosin gels when ATP is removed (*6*). The binding of monovalent anions to increase HMM and S1 negative charge is consistent with the results reported here, although Cl^- is present at trace levels and [$^-$OAc] is only 2.2 mM. It is not known if these monovalent ion concentrations are high enough to bind HMM.

Nucleotides and pyrophosphate bind to myosin at sites other than the active site, which could contribute to the low values of μ_e. When [Mg^{2+}] is low, two to three molecules of ADP, ATP, or AMPPNP bind to myosin, when the nucleotide concentration is in the 10 mM range (*46*). However, nonspecific nucleotide binding that is not coupled to active site occupancy is not consistent with the electric charge changes reported here for several reasons. The nucleotide concentrations used here (0.50−2.0 mM) are below the reported dissociation constant for nonspecific binding (>5 mM) (*46*). The number of nucleotides reported to bind, two to three per myosin (*46*), is too low to account for the observed net electric charge (Table 1). In addition, the free [Mg^{2+}] in the measurements reported here is 0.6 mM, high enough to eliminate nucleotide binding. The concentration dependence and stoichiometry of ATP and ADP binding are similar (*46*), whereas the increase in electrophoretic mobility is not observed in 1 or 2 mM ATP or in the presence of 0.5−2 mM ADP if ATP or ATPγS is bound in the active site. The dependence of the increase in net electric charge on the conversion of the steady-state intermediate to the ADP complex (Figures 4 and 5, Table 1) is strong evidence that if nonspecific nucleotide binding is involved, it is coupled to the P_i dissociation step of the hydrolytic cycle.

Two biological roles can be hypothesized for the nucleotide-induced motor domain electric charge changes. The first is based on intramolecular motor domain electrostatic repulsion. Because the largest increase in negative charge occurs when P_i dissociates, it is possible that increased electrostatic repulsion may contribute in some way to the power stroke that results when P_i dissociates from a motor domain bound to actin. To be more specific, the change from non-force-producing to force-producing motor domain state, which occurs before the lever arm rotates, may involve increased electrostatic repulsion between the catalytic and lever arm subdomains. The second possible role for the changes in net electric charge is the position of the cross-bridge relative to the thick and thin filaments. The closeness of the motor domains to both the thick and thin filaments (Figure 1) makes it likely that changes in electric charge would cause the motor domain to move.

REFERENCES

1. Rome, E. (1968) *J. Mol. Biol. 37*, 331−344.
2. Matsubara, I., and Elliott, G. F. (1972) *J. Mol. Biol. 72*, 657−669.
3. Millman, B. M., and Nickel, B. G. (1980) *Biophys. J. 32*, 49−63.
4. Wray, J. (1987) *J. Muscle Res. Cell Motil. 8*, 62.
5. Malinchik, S., Xu, S., and Yu, L. C. (1997) *Biophys. J. 73*, 2304−2312.
6. Bartels, E. M., Cooke, P. H., Elliott, G. F., and Hughes, R. A. (1993) *Biochim. Biophys. Acta 1157*, 63−73.
7. Berne, B. J., and Pecora, R. (1976) *Dynamic Light Scattering*, 1st ed., Wiley-Interscience, New York.
8. Molloy, J. E., Burns, J. E., Sparrow, J. C., Tregear, R. T., Kendrickjones, J., and White, D. C. S. (1995) *Biophys. J. 68*, S298−S305.
9. Rayment, I., Rypniewski, W. R., Schmidt-Base, K., Smith, R., Tomchick, D. R., Benning, M. M., Winkelmann, D. A., Wesenberg, G., and Holden, H. M. (1993) *Science 261*, 50−58.
10. Dominguez, R., Freyzon, Y., Trybus, K. M., and Cohen, C. (1998) *Cell 94*, 559−571.
11. Houdusse, A., Kalbokis, V. N., Himmel, D., Szentgyorgyi, A. G., and Cohen, C. (1999) *Cell 97*, 459−470.
12. Fisher, A., Smith, C. A., Thoden, J. B., Smith, R., Sutoh, K., Holden, H. M., and Rayment, I. (1995) *Biochemistry 34*, 8960−8972.
13. Gulick, A. M., Bauer, C. B., Thoden, J. B., and Rayment, I. (1997) *Biochemistry 36*, 11619−11628.
14. Gulick, A. M., Bauer, C. B., Thoden, J. B., Pate, E., Yount, R. G., and Rayment, I. (2000) *J. Biol. Chem. 275*, 398−408.
15. Smith, C. A., and Rayment, I. (1995) *Biochemistry 34*, 8973−8981.
16. Smith, C. A., and Rayment, I. (1996) *Biochemistry 35*, 5404−5417.
17. Cooke, R. (1997) *Physiol. Rev. 77*, 671−697.
18. Geeves, M. A., and Holmes, K. C. (1999) *Annu. Rev. Biochem. 68*, 687−728.
19. Highsmith, S. (1999) *Biochemistry 38*, 9791−9797.
20. Spudich, J. A. (2001) *Nat. Rev. Mol. Cell Biol. 2*, 387−392.
21. Warrick, H. M., Simmons, R. M., Finer, J. T., Uyeda, T. Q. P., Chu, S., and Spudich, J. A. (1993) *Methods Cell Biol. 39*, 1−21.
22. Mehta, A. D., Rock, R. S., Rief, M., Spudich, J. A., Mooseker, M. S., and Cheney, R. E. (1999) *Nature 400*, 590−593.
23. Trybus, K. M., Freyzon, Y., Faust, L. Z., and Sweeney, H. L. (1997) *Proc. Natl. Acad. Sci. U.S.A. 94*, 48−52.
24. Sellers, J. R. (1999) *J. Muscle Res. Cell Motil. 20*, 347−349.
25. Nauss, K. M., Kitagawa, S., and Gergely, J. (1969) *J. Biol. Chem. 244*, 755−765.
26. Weeds, A. G., and Taylor, R. S. (1975) *Nature 257*, 54−56.
27. Margossian, S. S., and Lowey, S. (1982) *Methods Enzymol. 85*, 55−71.
28. Kodama, T., Fukui, K., and Kometani, K. (1986) *J. Biochem. (Tokyo) 99*, 1465−1472.
29. Imamura, K., Tada, M., and Tonomura, Y. (1966) *J. Biochem. (Tokyo) 59*, 280−289.
30. Highsmith, S., Polosukhina, K., and Eden, D. (2000) *Biochemistry 39*, 12330−12335.
31. Tscharnuter, W. W., McNeil-Watson, F., and Fairhurst, D. (1996) in *Particle Size Distribution III, Assessment and Characterization* (Provder, T., Ed.) pp 327−340, American Chemical Society, Washington, DC.
32. Miller, J. F., Schatzel, K., and Vincent, B. (1991) *J. Colloid Interface Sci. 143*, 532−554.
33. Highsmith, S., and Eden, D. (1985) *Biochemistry 24*, 4917−4924.
34. Claire, K., Pecora, R., and Highsmith, S. (1997) *Biophys. Chem. 65*, 85−90.
35. Segel, I. H. (1975) *Enzyme Kinetics*, John Wiley & Sons, New York.
36. Highsmith, S. (1976) *J. Biol. Chem. 251*, 6170−6172.
37. Bagshaw, C. R., Eccleston, J. F., Trentham, D. R., Yates, D. W., and Goody, R. S. (1972) *Cold Spring Harbor Symp. Quant. Biol. 37*, 127−135.
38. Resetar, A. M., and Chalovich, J. M. (1995) *Biochemistry 34*, 16039−16045.
39. Mendelson, R. A., Morales, M. F., and Botts, J. (1973) *Biochemistry 12*, 2250−2255.
40. Overbeek, J. T., and Wiersma, P. H. (1967) in *Electrophoresis* (Bier, M., Ed.) pp 1−52, Academic Press, New York.
41. Allison, S. A., Potter, M., and McCammon, J. A. (1997) *Biophys. J. 73*, 133−140.
42. Basak, S. K., and Ladisch, M. R. (1995) *Anal. Biochem. 226*, 51−58.
43. Frank, G., and Weeds, A. G. (1974) *Eur. J. Biochem. 44*, 317−334.
44. Matsuda, G., Maita, T., Suzuyama, Y., Setoguchi, M., and Umegane, T. (1977) *J. Biochem. (Tokyo) 81*, 807−811.
45. Maita, T., Yajima, E., Nagata, S., Miyanishi, T., Nakayama, S., and Matsuda, G. (1991) *J. Biochem. (Tokyo) 110*, 75−87.
46. Harrington, W. F., and Himmelfarb, S. (1972) *Biochemistry 11*, 2945−2952.
47. Hunter, R. J. (1981) *Zeta Potential in Colloid Science: Principles and applications*, Academic Press Ltd., London.
48. Bartels, E. M., and Elliott, G. F. (1985) *Biophys. J. 48*, 61−76.

BI0202979